

Differences between Gaia DR2 and Gaia EDR3 photometry: demonstration, consequences, and applications

J. Maíz Apellániz¹ and M. Weiler²

¹ Centro de Astrobiología, CSIC-INTA, Spain

² Universitat de Barcelona, Spain

Abstract

We produce a new photometric calibration for the combined six-filter system formed by *Gaia* DR2 + EDR3 $G+G_{BP}+G_{RP}$ using an improved STIS/HST spectrophotometric library with very red stars. The comparison between observed and synthetic photometry yields residual dispersions of just 3.4-8.7 mmag, resulting in the most accurate and precise whole-sky large-dynamic-range optical photometric system ever obtained. We include some tests and applications.

1 Motivation and summary

Gaia has provided us with very stable, whole-sky, high-dynamic-range, optical photometry for over 10^9 stars but its full potential can only be achieved if we produce a calibration as free as possible of systematic effects and with uncertainties that allow for a true comparison between the observed magnitudes and synthetic photometry derived from SED models. In Maíz Apellániz & Weiler (2018) we obtained a photometric calibration for *Gaia* DR2 $G+G_{BP}+G_{RP}$ that was proven to be the most accurate one at that point. We have repeated the procedure for *Gaia* EDR3 with an improved spectrophotometric library and also reanalyzed the original *Gaia* DR2 system. The result is the most stable, accurate, and precise 6-filter optical photometry system ever achieved. There are significant differences between the DR2 and EDR3 photometric systems that can be exploited for scientific purposes.

2 Method

In Maíz Apellániz & Weiler (2018) we compiled a spectrophotometric stellar library from high-quality STIS G430L+G750L data for 122 stars with a broad range of colors and used the Weiler et al. (2018) technique to produce a full photometric calibration for *Gaia* DR2 $G+G_{BP}+G_{RP}$. In this contribution we have modified that list, eliminating some stars

Table 1: Calibration summary. Specific passbands are applicable only to the magnitude range and common ones are magnitude independent. Magnitude corrections can be global or applied only to saturated (very bright) stars. Z_{Vega} is the zero point for the passband in the Vega system. σ_0 is the minimum photometric uncertainty or value to add in quadrature to the catalog uncertainty when comparing observed magnitudes with synthetic photometry.

Band	Range (mag)	DR2				EDR3			
		passband	correction	Z_{Vega} (mag)	σ_0 (mmag)	passband	correction	Z_{Vega} (mag)	σ_0 (mmag)
G	$G < 13.00$	specific	yes	+0.036	6.5	specific	yes	+0.031	4.8
	$G > 13.00$	specific	yes	+0.041	5.1	specific	yes	+0.033	3.9
G_{BP}	$G < 10.87$	specific	no	+0.035	4.5	common	saturation	+0.020	3.8
	$G > 10.87$	specific	no	+0.022	5.3	common	no	+0.020	4.0
G_{RP}	$G < 10.87$	specific	no	+0.030	8.7	common	saturation	+0.022	5.7
	$G > 10.87$	specific	no	+0.023	5.1	common	no	+0.022	3.4

that were shown to have problems and, more importantly, adding stars from a dedicated STIS program (GO 15 816) to include additional very red stars: the previous list only had 3 stars with $2.9 < G_{\text{BP}} - G_{\text{RP}} < 4.8$ and none redder than that while the new one has 5 stars with $2.9 < G_{\text{BP}} - G_{\text{RP}} < 4.8$ and 4 redder than that. Including a significant number of very red stars is crucial in determining the red end of the G and G_{RP} passbands and most spectrophotometric libraries do not have them. As the *Gaia* population includes a significant fraction of very red stars (Fig. 1), most of them extinguished red giants and red clump stars, a calibration without such very red stars is likely to provide incorrect information about them. With that improved list in hand, we have recomputed the *Gaia* DR2 and EDR3 passbands for $G+G_{\text{BP}}+G_{\text{RP}}$ and produced a new photometric calibration for the 6-filter system. This contribution contains our preliminary results and the final results will appear in Weiler et al. (in preparation).

3 Magnitude ranges and corrections

In Maíz Apellániz & Weiler (2018) we computed **two G_{BP} DR2 bandpasses divided by G greater or smaller than 10.87 mag**, as we found out that the sensitivity was different in those two magnitude ranges. In our new analysis of DR2 we confirm this finding and **we add an equivalent division at the same G magnitude for G_{RP}** (Table 1 and Figs. 4 and 5). Furthermore, we have discovered that **the fit for the G band in both DR2 and EDR3 can be improved by adding a similar division at $G = 13.00$ mag** (Table 1), though in this case the differences between the bright and faint bandpasses are smaller than for G_{BP} or G_{RP} (Fig. 3). Therefore, a total of ten different bandpasses are needed to characterize the six-filter photometric system. The divisions in magnitude are likely caused by the use of TDI gates for the processing of *Gaia* CCD data (Prusti et al. 2016), so the origin is electronic and not optical.

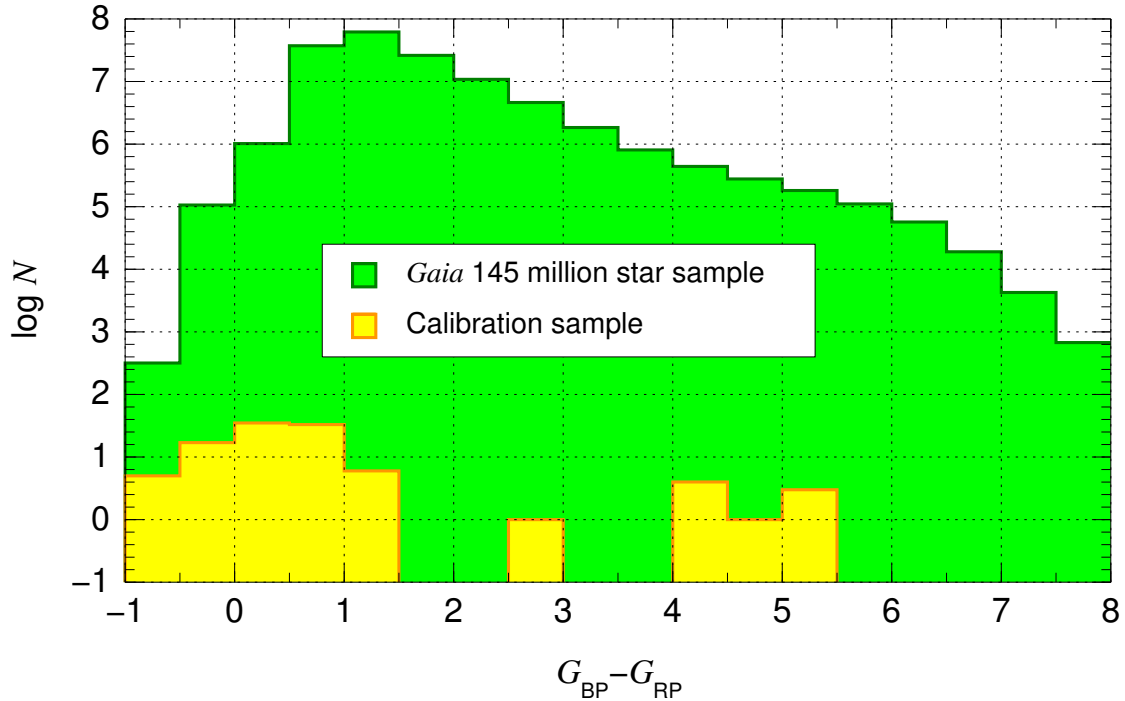


Figure 1: $G_{BP} - G_{RP}$ histograms for the *Gaia* 145 million star sample of Maíz Apellániz et al. (2023) and for the calibration sample in this contribution.

In Maíz Apellániz & Weiler (2018) we also included a **correction δG_2 for the G DR2 band** that led to corrected magnitudes $G'_2 = G_2 + \delta G_2$ (see also Arenou et al. 2018; Weiler 2018; Casagrande & Vandenberg 2018). We have recomputed the correction here and found a similar result (Fig. 2). Furthermore, we find that an equivalent correction is needed for the G EDR3 band (Fig. 2). For G_{BP} and G_{RP} we find that the EDR3 saturation corrections of Riello et al. (2021) (the results from their application may be called G'_{BP} and G'_{RP} , respectively) are sufficient.

4 Passband definitions and evolution

In Maíz Apellániz (2017) we discovered that the G DR1 passband was significantly redder than the nominal one from Jordi et al. (2010). This was likely caused by water freezing in some optical elements at the beginning of the mission (Prusti et al. 2016). In Maíz Apellániz & Weiler (2018) we detected that the G DR2 passband had become bluer, as the DR2 magnitudes were computed using a longer time baseline, and the effect of ice deposition had become less significant on average. Here we confirm the trend in time, as **for EDR3 the two G passbands are even bluer than their DR2 equivalents (Fig. 2).**

In Maíz Apellániz & Weiler (2018) we found out that the bright ($G < 10.87$ mag) G_{BP} DR2 passband was different from the faint ($G > 10.87$ mag) one, most significantly in its

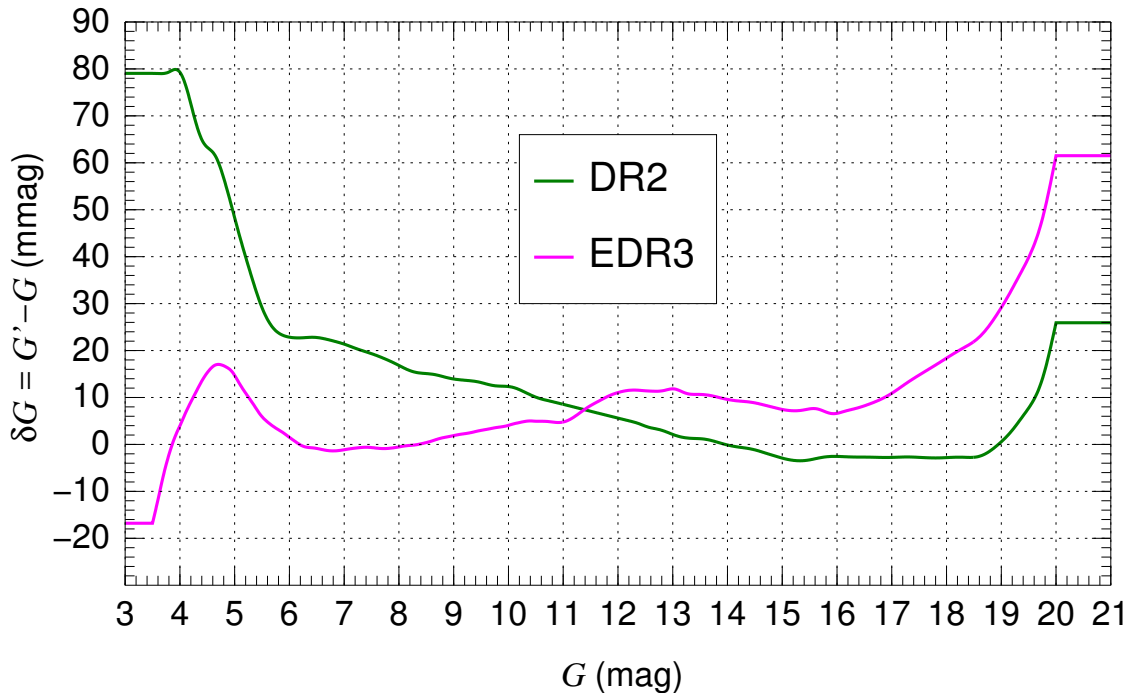


Figure 2: G corrections as a function of magnitude.

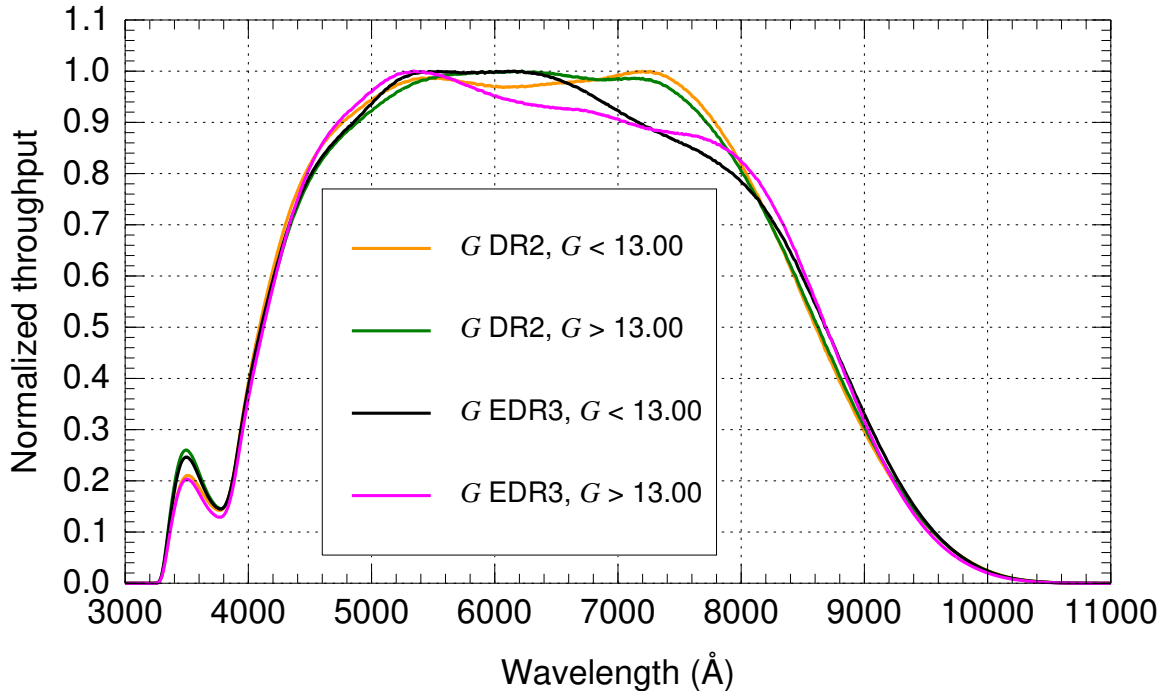
lower sensitivity to the left of the Balmer jump. Here we confirm that and we determine that the G_{BP} EDR3 passband is relatively similar to the bright DR2 one (and hence, significantly different from the faint one, Fig. 4). **The difference between the DR2 and EDR3 G_{BP} bandpasses for faint stars is important, given its scientific applications** (Figs. 7 and 8, see below).

The Maíz Apellániz & Weiler (2018) analysis did not include two passbands for G_{RP} in DR2 but the addition of very red stars to our new sample allows us to establish that they are indeed different, with the passband for faint ($G > 10.87$ mag) stars being significantly bluer than the one for bright stars. Furthermore, as we saw for G_{BP} , the G_{RP} EDR3 bandpass is relatively similar to the DR2 one for bright stars and significantly different from the DR2 one for faint stars. **The difference between the DR2 and EDR3 G_{RP} bandpasses for faint stars can also be exploited**, as it is sensitive in different degrees to broad-band colors in the 7000-9000 Å region and to $H\alpha$.

5 Accuracy and precision

In the two previous sections we have described the corrections that have to be applied to the observed G photometry, the magnitude ranges in which each filter has to be divided, and the respective passbands. Two final steps are required for a meaningful comparison between the observed photometry and the synthetic one obtained from SED models.

First, a Vega zero point, Z_{Vega} , has to be determined for each passband (Table 1) in

Figure 3: *G* passbands.

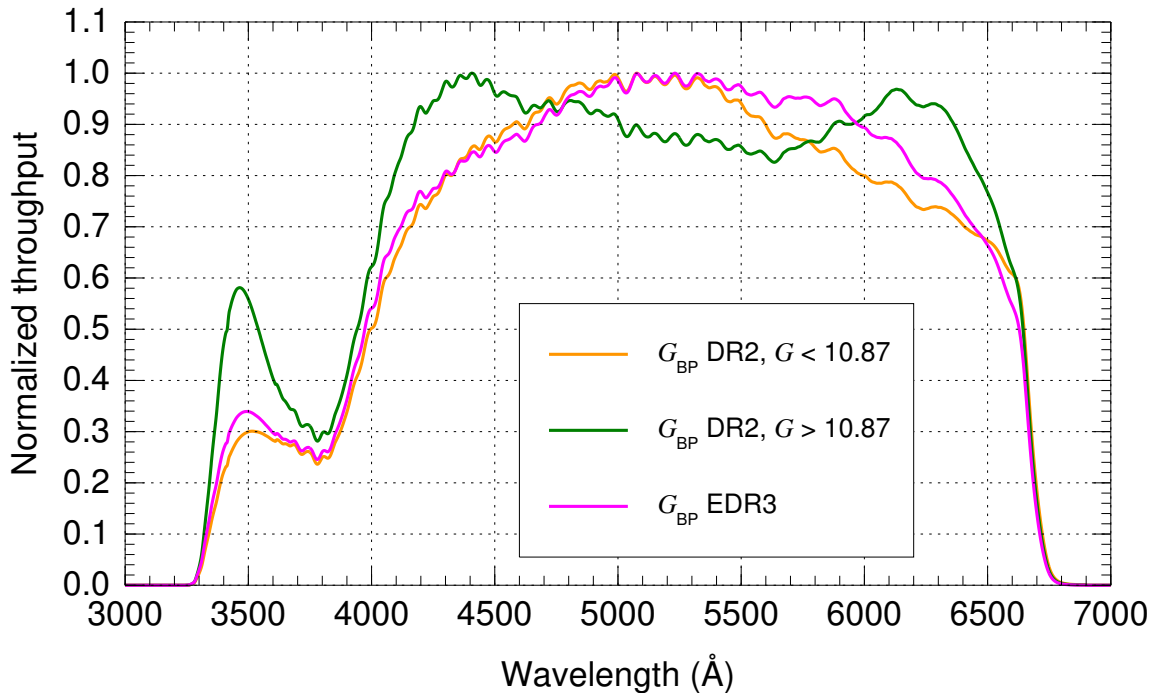
order for accurate synthetic magnitudes to be obtained through:

$$m_{\text{syn}} = -2.5 \log_{10} \left(\frac{\int P(\lambda) F_{\lambda}(\lambda) \lambda d\lambda}{\int P(\lambda) F_{\lambda, \text{Vega}}(\lambda) \lambda d\lambda} \right) + Z_{\text{Vega}}, \quad (1)$$

see Maíz Apellániz (2024) for definitions and details. In particular, we adopt the Vega SED `alpha_lyr_stis_010.fits` from CALSPEC (Bohlin 2014).

Second, the overall precision of the calibration has to be established by determining the minimum photometric uncertainty σ_0 to be combined with the observed photometric uncertainties σ to generate the corrected uncertainties $\sigma' = \sqrt{\sigma^2 + \sigma_0^2}$. The corrected uncertainties are the relevant ones for a comparison between observed and synthetic magnitudes and include the uncertainties in our knowledge of the passbands and other peculiarities of the photometric system. They are calculated by comparing the (assumed exact) synthetic magnitudes from HST spectrophotometry with the observed magnitudes divided by the corrected uncertainties and forcing the resulting distribution to have a standard deviation of one (the mean is already forced to be zero by the calibration itself).

The values of σ_0 are very low (Table 1), ranging from 4.5 mmag to 8.7 mmag for DR2 and from 3.4 mmag to 5.7 mmag for EDR3. They are significantly lower than their equivalents for other photometric systems (Maíz Apellániz 2006), thus **establishing *Gaia* as the the most precise whole-sky large-dynamic-range optical photometric system ever obtained**. Furthermore, the improvement in the calibration from DR2 to EDR3 is noticeable in the reduction of the σ_0 values.

Figure 4: G_{BP} passbands.

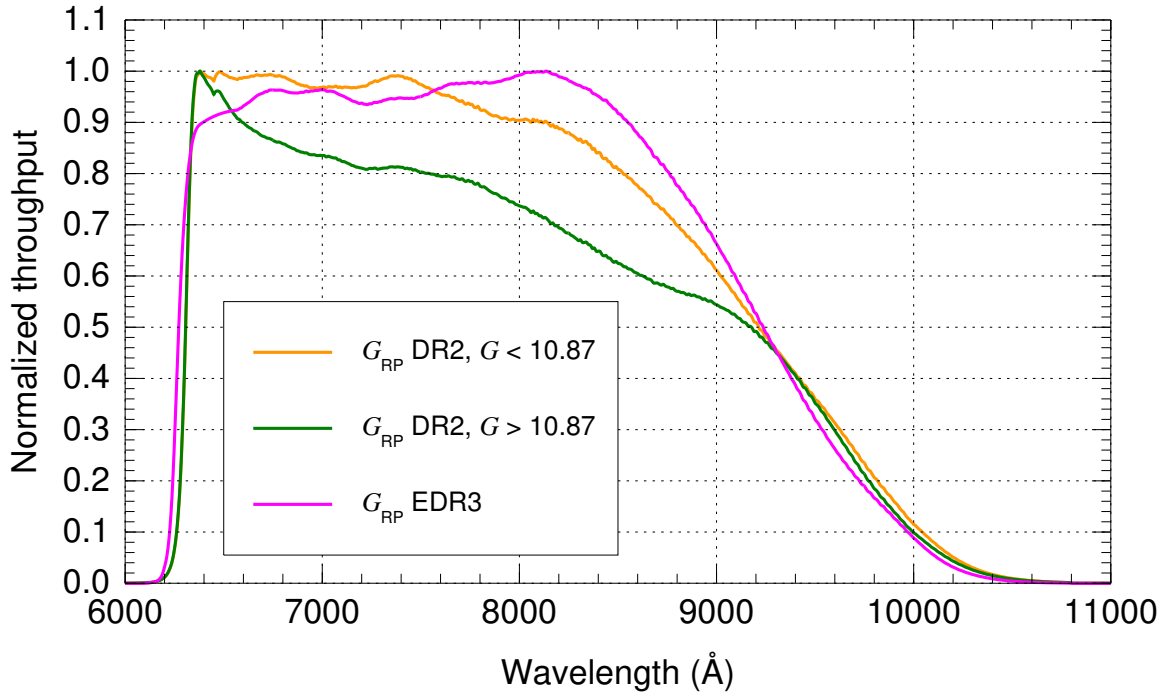
6 Testing and applications

We tested our passbands with a large sample of OB stars from the ALS project (Pantaleoni González et al. 2021; 2024 in preparation) and synthetic photometry computed with the SED grid of Maíz Apellániz (2013). The use of OB stars allows us to select targets with similar intrinsic SEDs (with the main difference being at the left of the Balmer jump) modified by different levels of extinction to generate observed SEDs of different colors.

First, we plot the difference between the EDR3 and DR2 G magnitudes as a function of $G_{\text{BP}} - G_{\text{RP}}$ using both uncorrected and corrected magnitudes (Fig. 6). The corrections significantly reduce the dispersion, confirming their validity. In addition, the distribution follows the function expected from the synthetic photometry of extinguished OB stars, confirming the validity of the passbands.

In Fig. 7 we plot the difference between the EDR3 and DR2 G_{BP} magnitudes as a function of $G_{\text{BP}} - G_{\text{RP}}$ dividing the sample in four according to two criteria: G brighter or fainter than $G = 10.87$ mag and spectral classification as O or B (with the latter including a small number of sdO stars). In that plot:

- Bright stars ($G < 10.87$ mag) follow a nearly constant trend in color, as predicted by the synthetic photometry of stars with T_{eff} in the 10-50 kK range. The explanation is that the G_{BP} bright DR2 and EDR3 passbands are very similar (Fig. 4), with an offset created by the different zero points (Table 1).

Figure 5: G_{RP} passbands.

- Faint stars ($G > 10.87$ mag), on the other hand, have a significant dependence with color, also in accordance with the synthetic photometry. This is explained by the difference between the G_{BP} faint DR2 and EDR3 passbands (Fig. 4): the former is more sensitive for $\lambda < 4700$ Å, especially for the region around 3500 Å that lies to the left of the Balmer jump. For hot stars with low extinction, a significant fraction of the flux comes from that region, causing the DR2 magnitude to be brighter than the EDR3 one in Fig. 7. As OB stars become more extinguished, the contribution from that wavelength region becomes less important and the two magnitudes become similar.
- Another effect for the faint range is that for highly extinguished OB stars ($G_{\text{BP}} - G_{\text{RP}} > 2.0$ mag) the above trend is reversed and DR2 G_{BP} magnitudes become once again brighter than EDR3 ones. This also has an explanation in Fig. 4. At the red end of the filter ($\lambda > 6000$ Å), the faint DR2 passband becomes more sensitive than the EDR3 one. When OB stars are highly extinguished, a significant fraction of the flux originates in that part of the passband, causing the effect.

In Fig. 8 we plot only the faint OB stars in Fig. 7 and we also add a sample of later-type objects dominated by A stars. There we see a significant T_{eff} trend, with hotter stars being brighter in DR2 than in EDR3 for a given $G_{\text{BP}} - G_{\text{RP}}$ color. The trend is more marked at low extinction, as the effect of the flux to the left of the Balmer jump is stronger there (see above) and eventually disappears at very high extinction (note that there are more low-extinction B stars than the equivalent of O type, a well known effect among Galactic bright stars).

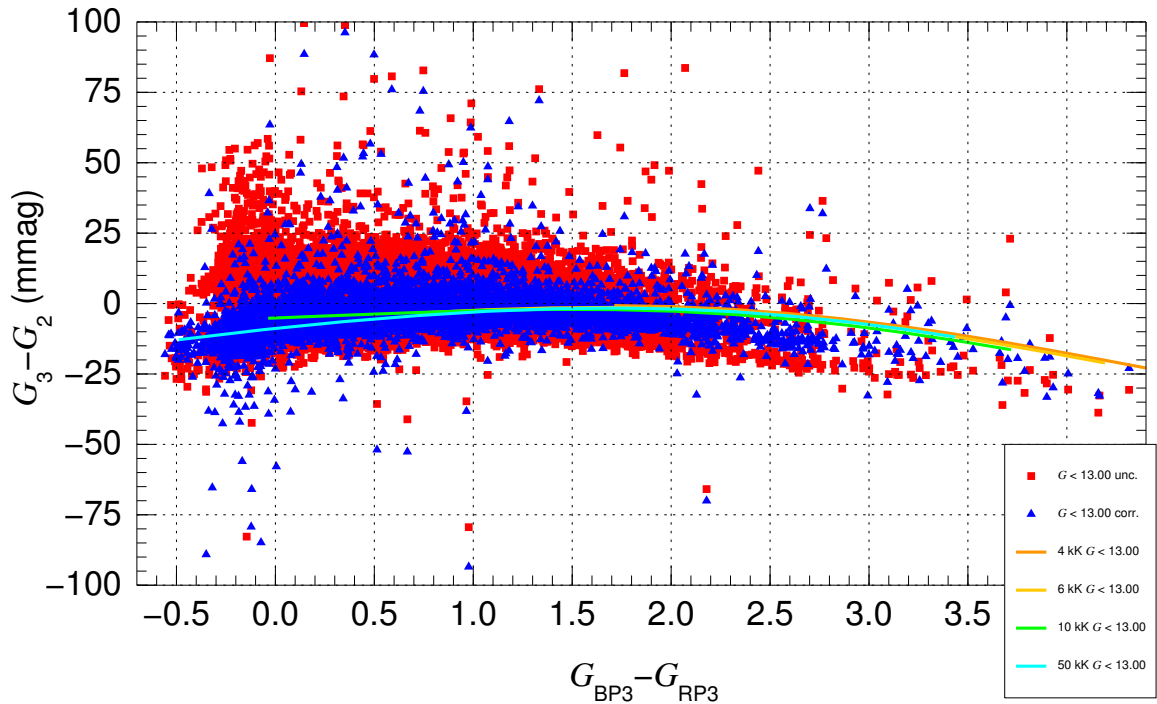


Figure 6: ΔG between EDR3 and DR2 as a function of $G_{\text{BP}} - G_{\text{RP}}$ for the ALS+ sample with $G < 13.00$ using uncorrected (red) and corrected (blue) magnitudes. The lines show the extinction tracks (Maíz Apellániz et al. 2014) for MS stars of different T_{eff} .

Therefore, **it is possible to use the *Gaia* six-filter system to estimate T_{eff} among OBA stars** in a manner analogous to classical Johnson $U - B$ versus $B - V$ diagrams.

A test of the quality of the calibration can be done using the SED-fitting code CHORIZOS (Maíz Apellániz 2004), which has been adapted to include it. We have applied it to several OB stars of different degrees of extinction in Maíz Apellániz et al. (2024) and in poster P252 in these proceedings (Maíz Apellániz & Negueruela 2025) in combination with 2MASS JHK photometry to produce a nine-degree filter system and simultaneously derive the extinction parameters and the luminosity. The resulting fits are excellent, with χ_{red} values close to 1.0, something that can only happen if the calibration, intrinsic SEDs, and extinction laws are all simultaneously accurate (Maíz Apellániz 2024).

7 Data availability

We have integrated our analysis into an IDL package called Gaiasoft that downloads *Gaia* data from Vizier, introduces the necessary corrections, plots the passbands, and computes the synthetic photometry. It will be released when Weiler et al. is published. In the meantime, contact the main author at jmaiz@cab.inta-csic.es for conditions on its use.

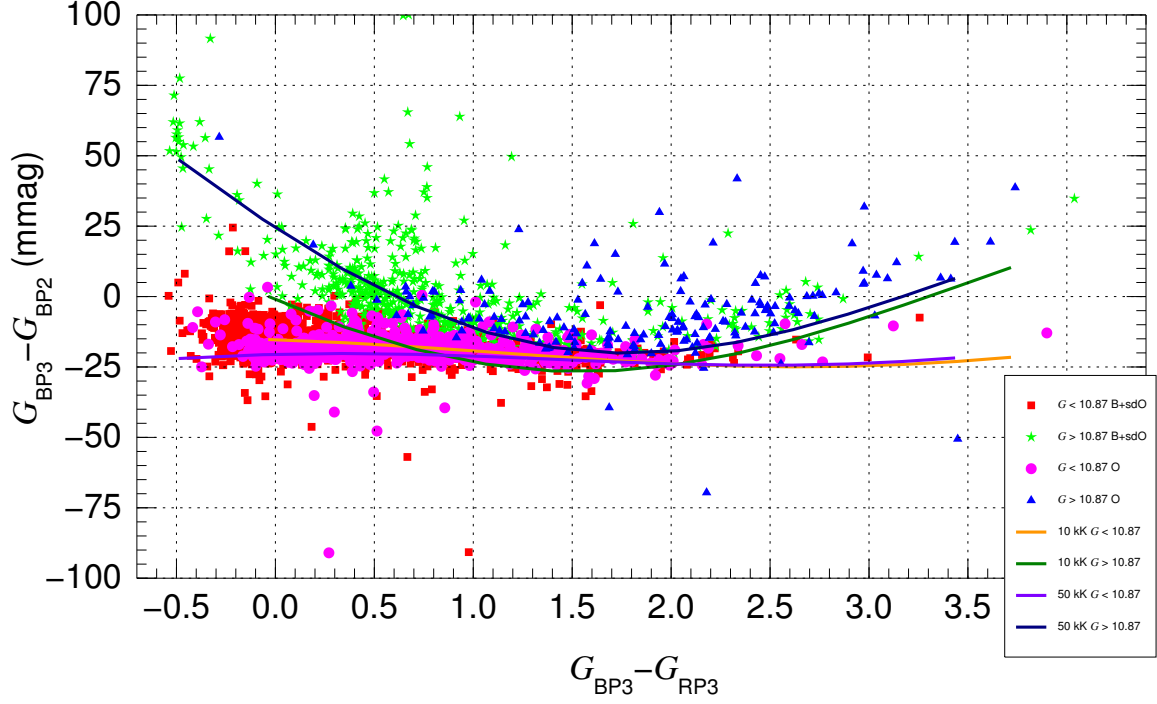


Figure 7: ΔG_{BP} between EDR3 and DR2 as a function of $G_{\text{BP}} - G_{\text{RP}}$ for the ALS+ early-type samples. The lines show the extinction tracks for MS stars of different T_{eff} .

References

- Arenou, F., Luri, X., Babusiaux, C., et al. 2018, *A&A*, 616, A17
- Bohlin, R. C. 2014, *AJ*, 147, 127
- Casagrande, L. & VandenBerg, D. A. 2018, *MNRAS*, 479, L102
- Jordi, C., Gebran, M., Carrasco, J. M., et al. 2010, *A&A*, 523, A48+
- Maíz Apellániz, J. 2004, *PASP*, 116, 859
- Maíz Apellániz, J. 2006, *AJ*, 131, 1184
- Maíz Apellániz, J. 2013, in *Highlights of Spanish Astrophysics VII*, 657–657
- Maíz Apellániz, J. 2017, *A&A*, 608, L8
- Maíz Apellániz, J. 2024, arXiv:2401.01116
- Maíz Apellániz, J., Evans, C. J., Barbá, R. H., et al. 2014, *A&A*, 564, A63
- Maíz Apellániz, J. & Negueruela, I. 2025, in *Highlights of Spanish Astrophysics XIII*, P252 (these proceedings), arXiv:2407.20812

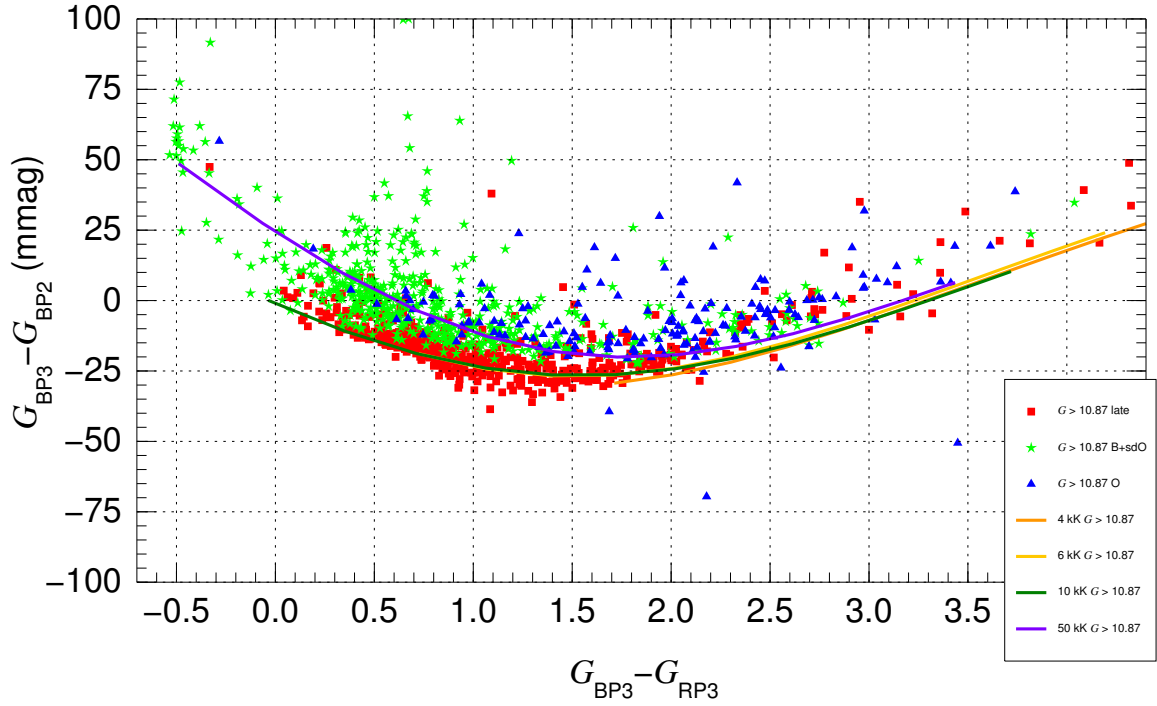


Figure 8: ΔG_{BP} between EDR3 and DR2 as a function of $G_{BP} - G_{RP}$ for the ALS+ sample with $G > 10.87$. The lines show the extinction tracks for MS stars of different T_{eff} .

Maíz Apellániz, J. & Weiler, M. 2018, A&A, 619, A180

Maíz Apellániz, J., Youssef, A. R., El-Nawawy, M. S., et al. 2024, arXiv:2405.13395

Maíz Apellániz, J. et al. 2023, A&A, 677, A137

Pantaleoni González, M., Maíz Apellániz, J., et al. 2021, MNRAS, 504, 2968

Prusti, T., de Bruijne, J. H. J., Brown, A. G. A., et al. 2016, A&A, 595, A1

Riello, M., De Angeli, F., Evans, D. W., et al. 2021, A&A, 649, A3

Weiler, M. 2018, A&A, 617, A138

Weiler, M., Jordi, C., Fabricius, C., & Carrasco, J. M. 2018, A&A, 615, A24